Modular Design for Acoustic Metamaterials: Low-Frequency Noise Attenuation

Lingling Wu, Zirui Zhai, Xinguang Zhao, Xiaoyong Tian, Dichen Li, Qianxuan Wang, and Hanqing Jiang*

A modular design method is introduced to design an acoustic metamaterial based on nested Helmholtz resonators that target low-frequency sound attenuation. The method combines a performance evaluation using finite element methods with structural evolution, and uses a genetic algorithm to optimize the acoustic metamaterial to attain the desired properties. Both the simulated and experimental results demonstrate the noise attenuation property of the optimized acoustic metamaterials. The modular design method proposed by this study may potentially design acoustic metamaterials for practical sound attenuation applications in industries by considering different environments and constraints.

1. Introduction

Acoustic metamaterials are artificially constructed structures that manipulate the propagation of acoustic energy, such as, acoustic cloaking,[1,2] negative refraction,[3] subwavelength imaging,[4,5] and sound attenuation.[6] Many notable results have been achieved, including mass-in-mass structures, membrane-type structures,[7–9] and Helmholtz

L. Wu, X. Tian, D. Li
State Key Laboratory for Manufacturing Systems Engineering
Xi'an Jiaotong University
Xi'an 710049, China
Z. Zhai
School for Engineering of Matter
Transport and Energy
Arizona State University
Tempe, AZ 85287, USA
X. Zhao
Liaoning Engineering Research Center of Health Monitoring and
Maintenance Technology for Large Mechanical Equipment
Liaoning Institute of Science and Technology
Mingshan District, Benxi 117004, China
Q. Wang
College of Railway Engineering
Wuyi University
Jiangmen 529020, China
H. Jiang
School of Engineering
Westlake University
Hangzhou 310024, China
E-mail: hanqing.jiang@westlake.edu.cn

The ORCID identification number(s) for the author(s) of this article can be found under https://doi.org/10.1002/adfm.202105712.

cavity resonators.[10,11] The many applications of acoustic metamaterials include super resolution acoustic imaging,[12,13] acoustic cloaking,[1,2,14] and acoustic waves steering;[15–17] however, airborne noise attenuation is one of the most important applications. Noise pollution is the second most significant environmental risk to our health,[18] both physiological[19] and psychological.[20] Noise policies have been implemented by various governmental agencies (e.g., European Environment Agency and United States Environmental Protection Agency) and the World Health Organization; the policies typically include three factors: the source of the noise, the transmission path, and the protection at the receiver's site. Without regarding the source of the noise, typical noise suppression methods target the transmission path and receiver's site, and they can be characterized into passive control and active control.[21,22] Active methods detect the original sound source and generate a secondary sound wave that results in destructive interference with the primary one. This method is efficient under most conditions, even for low-frequency sound, which is known to have a long penetrating power and a greater influence on health.[23] However, most active noise reduction systems are complex and require considerable electrical power.[23] On the contrary, passive methods are more accessible and robust, and they are low-cost.

Among the passive methods, the Helmholtz resonator (HR),[10,24–35] which utilizes a cavity structure as a basic acoustic resonant model, has been extensively studied to achieve low-frequency bandgaps for noise attenuation. However, this type of resonator is only effective at its single resonance peak with a narrow frequency band.[36,37] An extended neck or spiral neck has been used to replace the traditional straight neck of the HR to improve its noise attenuation performance[36] at low frequencies within a limited space. Despite these efforts, a general design to construct HRs with a desired acoustic performance has not yet been developed. With the development of machine learning, various structures with predetermined properties may be automatically determined; thus, it provides a powerful tool to simplify the metamaterials design process.

In this study, we adopted a genetic algorithm (GA) to search for the optimal meta-atom that has a maximized first relative bandgap, which is proven to be an effective method to control low frequency noise. The developed modular design method is easier to operate and less time-consuming than existing

metamaterial designing methods, such as, topology optimization, trial and error, and so on. Therefore, it is generally applicable to metamaterial design, which is rarely investigated by previous research work. Theoretical and experimental studies were conducted to quantify the sound attenuation performance of the optimized acoustic metamaterials. The results showed that the optimized acoustic metamaterials outperformed the sound barriers that were made of the same material. The optimized acoustic metamaterials may also be applied in industry, including highway sound barriers and noise reduction in airports and factories.

2. General Methodology of the Modular Design Method

The modular design method consists of two parts, namely, the finite element analysis that evaluates the performance of the meta-atom candidates and the GA model that creates the design based on the performance of these meta-atoms. The aim is to determine the optimal meta-atom with the desired acoustic properties. The schematic of the GA process is shown in Figure S1, Supporting Information, and the brief operation process is as follows. The genetic algorithm will randomly generate a number of initial values for the 12 variables, in which each set of the 12 variables represents a candidate structure of the problem. By evaluating the acoustic performance of corresponding structure through finite element analysis,

the algorithm could gradually evolve, which is the "structural evolution." The population size depends on the number of design variables, meaning that the more design variables, the larger the population size. Then, the GA is employed to determine the optimal solution by genetically breeding a population of individuals over a series of generations until the change of the fitness function between two adjacent generations is smaller than the tolerance.[38] Through sequential iteration and the structural evolution, a meta-atom with an optimal arrangement of structural bases is thus achieved. Here, COMSOL Multiphysics was used for the finite element simulation, and it can be readily combined with the GA model via LiveLink for MATLAB.

3. Optimization of the Nested Helmholtz Resonator

A nested Helmholtz resonator with 4 layers of concentrically C-shaped resonators[39–41] was considered in this study, as shown in **Figure 1**a. Based on existing studies (e.g., ref. [29]), the C-shaped Helmholtz resonator has low-frequency bandgaps. The component for each layer is white polyvinyl chloride pipes (modulus = 3.2 GPa, density = 1380 kg m^{-3}), and the rings are confined in a 100×100 mm square. As shown in Figure 1a, there are 12 to-be-optimized parameters: the thickness of each layer T_1, T_2, T_3, and T_4; the gap width of each layer D_1, D_2, D_3, and D_4; and the rotating angle of the gap α_1, α_2,
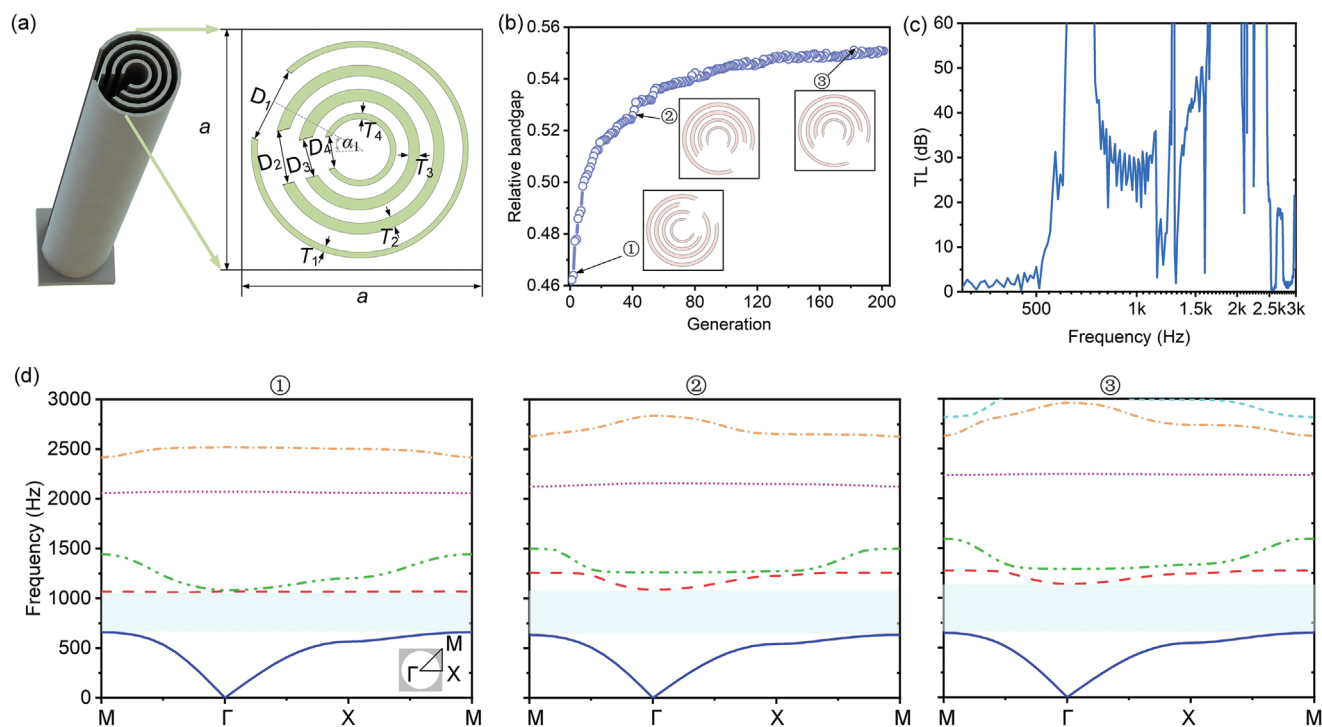
Figure 1. Modular design method to design an acoustic meta-atom. a) Design model of a nested Helmholtz resonator with 12 to-be-optimized parameters (only 9 shown here). b) Optimization iteration history by applying GA, where insets ①, ②, and ③ show the best configuration of the 2nd, 40th, and 182th generation, respectively. c) The transmission loss of an acoustic metamaterial constructed by 20 layers of optimal meta-atoms. d) The bandgap structures of meta-atoms ①, ②, and ③ shown in (b).

α_3, and α_4 (not shown in Figure 1a). The periodicity a_1 of the simulated models equates to 100 mm, and the outside radius of the largest circular inclusion R_1 is set as 45 mm. The values of R_2, R_3, and R_4 are 37.5, 25, and 20 mm, respectively, to avoid the geometrical overlap of each layer and guarantee fabrication feasibility during the optimization process of each parameter. The population size of the GA is 100; thus, there are 100 finite element simulations in each generation to evaluate the band structure. The details of the GA optimization (Figure S1, Supporting Information) and the searching constraints of the parameters are presented in Supporting Information.

For a given structure, the jth bandgap was calculated using the difference between the maximized value of the jth band and the minimum value of the $(j+1)$th band. The jth relative width of the bandgap was then defined as the ratio between the width of the jth bandgap and its corresponding midgap frequency (i.e., the average bandgap of the jth and $(j+1)$th bands). In the optimization, the 1st relative width of the bandgap was adopted as the fitness function f_1:

$$f_1 = \max \left\{ \frac{\min(\omega_2) - \max(\omega_1)}{\frac{\min(\omega_2) + \max(\omega_1)}{2}} \right\} \tag{1}$$

where ω_1 and ω_2 are the frequencies of the first and second bands, respectively.

The GA calculation process is shown in Figure 1b, from which it can be observed that a maximized fitness function value of 0.55 was obtained in the 182th generation. Given that there are 100 populations in each generation, a relatively large amount of finite element simulations is required to achieve the optimized configuration, which demonstrates the efficiency of this modular design method. The structure of the optimal meta-atom with a relative bandgap of 0.55 is shown in the inset of Figure 1b. The optimal parameters are included in Supporting Information. Figure 1d presents the bandgap structure of configurations ①–③, which are marked in Figure 1b; the figure shows that the complete bandgap becomes wider and lower during the iteration process. The optimal configuration ③ presents a wide complete bandgap between 649.1 and 1140.6 Hz. Based on this meta-atom, an acoustic metamaterial with a maximized relative bandgap can be constructed. The transmission loss (TL) of a finite array model with 20 layers of meta-atoms is shown in Figure 1c. The simulation direction is Γ-X, and a larger bandgap, from 547.6 to 1140.6 Hz, is obtained. Figure S2, Supporting Information, provides the sound pressure level in dB of the 3-layer metamaterial at several representative frequencies. It exhibits a distinguishable sound pressure drop in the bandgap region.

4. Experimental Verification and Discussion

Due to the cost constraint, only the optimal acoustic metamaterial sample was fabricated. **Figure 2**a–c illustrates the experimental setup used to test the sound attenuation performance of the sample, where three layers of the optimized nested Helmholtz resonators were placed between a sound source and a receiver. The distance between the receiver and sample equals to that between the sample and sound source, which are indicated by d. Figure 2b shows a photograph of the experimental setup in an anechoic chamber, where the three layers of nested Helmholtz resonators are 3.3 m in width, 2.2 m in height, and 0.3 m in depth. The metamaterial reaches the ceiling of the anechoic chamber to be consistent with the simulation. The wall and ceiling of the anechoic chamber is covered with sound absorbing materials to ensure an accurate measurement. Further details of the noise source and instruments are presented in Supporting Information.

The TL of the acoustic metamaterial when $d = 0.8$ m is shown in Figure 2d. The aim of the optimization process was to maximize the 1st relative bandgap; thus, it is clear that the optimized metamaterial exhibits a great sound attenuation performance, particularly in the low-frequency range (e.g., from 547.6 to 1140.6 Hz). To quantify the sound attenuation performance of the acoustic metamaterial, we defined a quality factor TL_{avg} as the average transmission loss between 649.1 and 1140.6 Hz (because this is the optimization frequency region), which is given by

$$TL_{avg} = \frac{\int_{649.1\,Hz}^{1140.6\,Hz} TL df}{1140.6\,Hz - 649.1\,Hz} \tag{2}$$
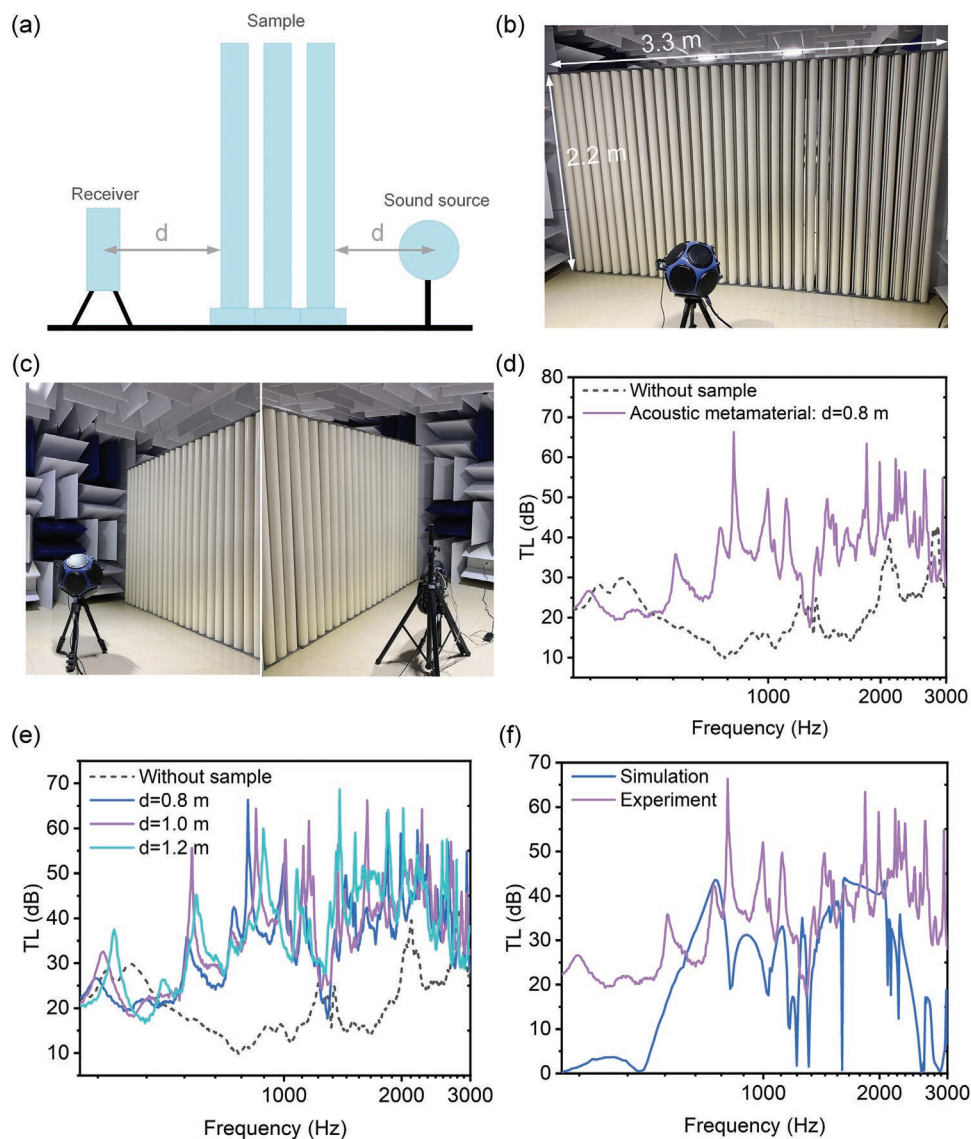
where TL refers to the transmission loss from Figure 2d, which is calculated by:

$$TL = -10 \lg \left(\frac{P_{out}}{P_{in}} \right) \tag{3}$$

where TL is the transmission loss in dB, P_{out}, and P_{in} are the transmitted and incident power, respectively.

Figures 2e shows the experimental results for different distance d, which shows a very slight shift of the peak to higher frequency domain when d increases. Videos S1–S3 presented the recorded sound pressure level at the receiver side ($d = 1$ m) without acoustic metamaterial, with perfect 3-layer acoustic metamaterial, and with defective 3-layer acoustic metamaterial, respectively. The TL_avg of the acoustic metamaterial are 37.9, 38.8, and 38.1 dB for $d = 0.8$, 1.0, and 1.2 m, respectively. Figure 2f compares the experimental and simulated results of the transmission loss using the optimized acoustic metamaterials at distance $d = 0.8$ m. It is found that the TL_avg values are fairly close though some discrepancies still exist, with 30.6 dB for the simulation and 37.9 dB for the experiments.

There are several factors that may lead to these discrepancies. The smoother transmissibility curve in the simulations, relative to the "noisy" transmission loss from the experiments, is due to fabrication defects.

The optimized acoustic metamaterial also exhibits a thickness effect in terms of the number of layers. Theoretically, the optimized acoustic metamaterial has a complete bandgap between 649.1 and 1140.6 Hz (see ③ in Figure 1d). Even a 20-layer acoustic metamaterial has a great transmission loss in the same frequency range (Figure 1c). Practically, only a very limited number of layers can be applied, owing to either cost

**ADVANCED
SCIENCE NEWS**
www.advancedsciencenews.com
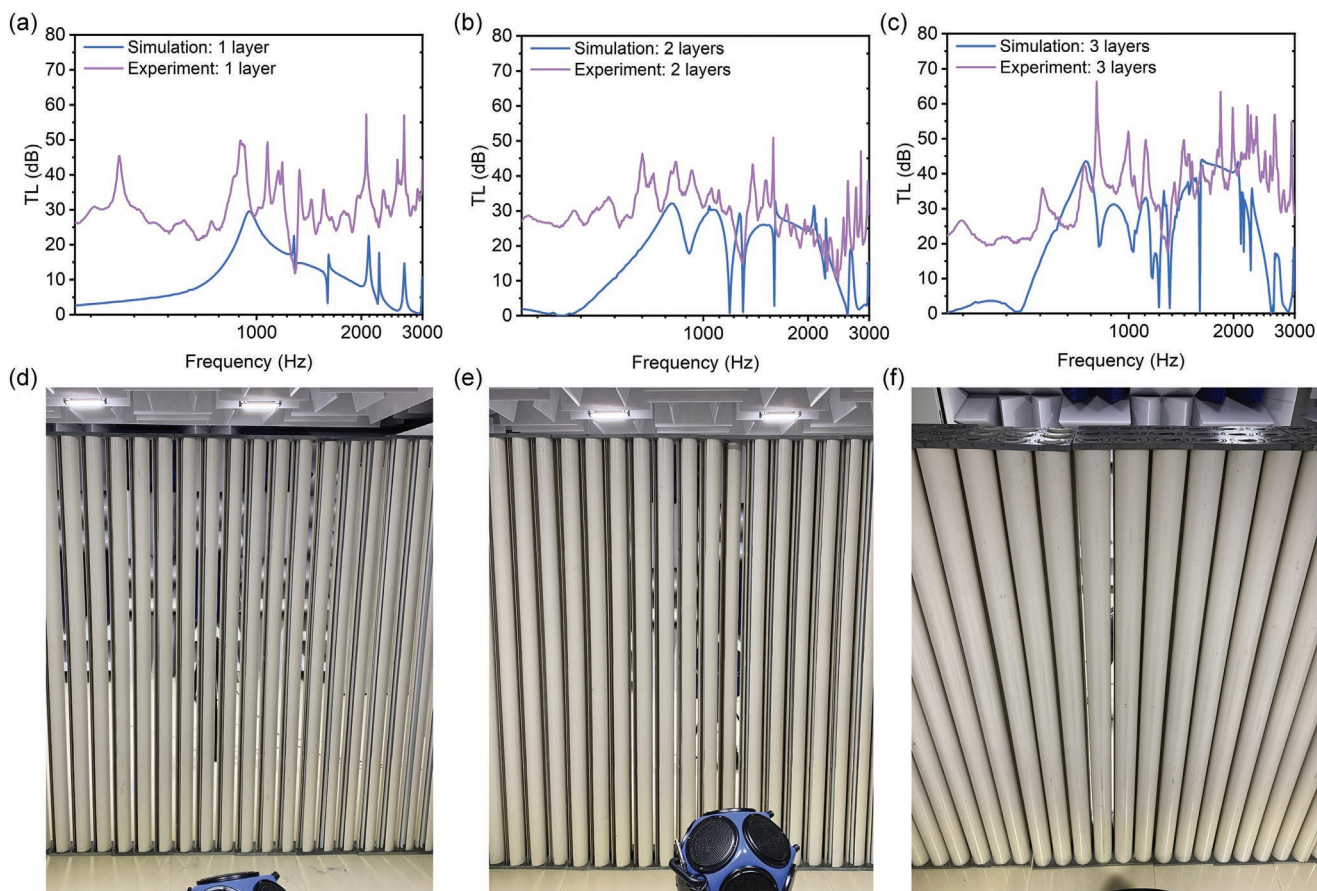
**ADVANCED
FUNCTIONAL
MATERIALS**
www.afm-journal.de

Figure 2. Experimental setup and measurement results. a) Schematic of the experimental setup. b,c) Experimental setup for a 3-layer acoustic metamaterial. d) Comparison of measurement results with and without acoustic metamaterial. e) Comparison of experimental results for different (d). f) Comparison of simulated and experimental results of the 3-layer acoustic metamaterial.

or size considerations. To evaluate the effect of the number of layers on the sound attenuation, the transmission losses for 1-layer, 2-layer, and 3-layer acoustic metamaterials were measured at $d = 0.8$ m, and the results were compared with that of the simulations (**Figure 3**). Figure 3 shows that with an increase in the number of layers, both the simulation and experiment start to exhibit a larger transmission loss over the desired frequency range, and a smaller discrepancy between the simulations and experiments appears.

Another practically important factor is the acoustic metamaterials' robustness to defects in terms of the performance of sound attenuation. We have intentionally removed 1 element from a perfect acoustic metamaterial (**Figure 4**a). Figure 4b shows the simulated result of a 3-layer acoustic metamaterial with and without defects, from which it can be observed that

the influence of the defects is relatively small. The experimentally measured TL_avg values are 36.8 and 37.9 dB with and without defects ($d = 0.8$ m), respectively, which exhibits only a marginal difference (Figure 4c). Figure 4d,e show the comparison of experimental results between sample with and without defects for $d = 1.0$ and 1.2 m, respectively. Figure 4f,g present the simulated sound pressure level at 2000 Hz for the metamaterial with and without defects, respectively. From the comparison of the results, we could conclude that the influence of defects on the performance of acoustic metamaterials is very small, which demonstrates that the performance of acoustic metamaterials is relatively robust.

We also carried out another three GA calculations to verify the convergence of optimization results (see Figure S3, Supporting Information). From the results, one can see that

**ADVANCED
SCIENCE NEWS**
www.advancedsciencenews.com

**ADVANCED
FUNCTIONAL
MATERIALS**
www.afm-journal.de

Figure 3. Investigation of the influence of the number of layers on the performance of the acoustic metamaterial. Comparison of experimental and simulated results of the acoustic metamaterial with a) 1 layer, b) 2 layers, and c) 3 layers. Experimental set up for the metamaterial with d) 1 layer, e) 2 layers, and f) 3 layers.

the optimization result show little dependence on the GA calculation process, which is very important in practical application, especially when the number of optimized parameters is very large.

5. Conclusion

Here, a modular design-based method for the design of acoustic metamaterials with low-frequency sound attenuation performance was introduced. The method combines performance evaluation with structural evolution to construct an acoustic metamaterial. Although the present study focuses on the sound attenuation in the low frequency range, the modular design method can be applied to design acoustic metamaterials in different frequency ranges by customizing the fitness function. Both the simulated and experimental results are provided to demonstrate the noise attenuation property of the optimized acoustic metamaterial. Given the practical limitations of the fabrication accuracy and experiments situation, such as, cost and size, the experiments do not replicate the simulation. With the development of manufacturing technology, the limitations mentioned above could be overcome. It is believed that the modular design method presented in this study has the potential to design acoustic metamaterials for practical sound attenuation in industries by considering different environments and constraints.
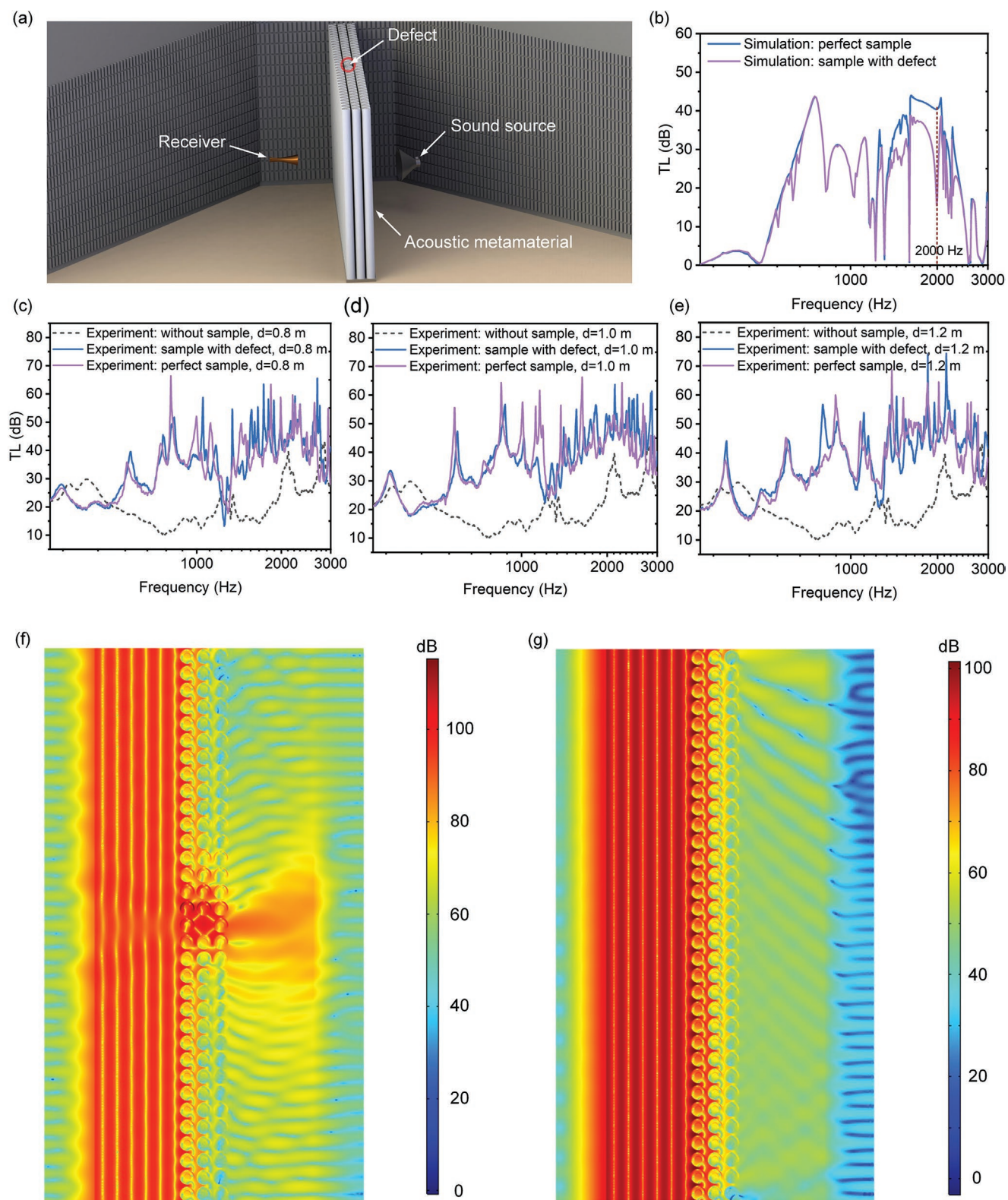
Supporting Information

Supporting Information is available from the Wiley Online Library or from the author.

Acknowledgements

Conflict of Interest

The authors declare no conflict of interest.

ADVANCED
SCIENCE NEWS

www.advancedsciencenews.com

ADVANCED
FUNCTIONAL
MATERIALS

www.afm-journal.de

Figure 4. Effect of defect on the performance of acoustic metamaterial. a) Schematic of the setup to test the metamaterial sample with 1 defect in the middle of the second layer. b) Simulated results for a 3-layer acoustic metamaterial with and without defect. c–e) Experimental results for a 3-layer acoustic metamaterial with and without defect when d equals to 0.8, 1.0, and 1.2 m, respectively. f,g) Simulated acoustic pressure level at 2000 Hz for a 3-layer acoustic metamaterial with and without defect, respectively.

Data Availability Statement

The data that support the findings of this study are available from the corresponding author upon reasonable request.

[1] V. M. García-Chocano, L. Sanchis, A. Díaz-Rubio, J. Martínez-Pastor, F. Cervera, R. Llopis-Pontiveros, J. Sánchez-Dehesa, *Appl. Phys. Lett.* **2011**, *99*, 074102.

[2] L. Zigoneanu, B.-I. Popa, S. A. Cummer, *Nat. Mater.* **2014**, *13*, 352.

[3] J. Li, C. T. Chan, *Phys. Rev. E* **2004**, *70*, 055602.

[4] Y. Xie, B.-I. Popa, L. Zigoneanu, S. A. Cummer, *Phys. Rev. Lett.* **2013**, *110*, 175501.

[5] J.-F. Robillard, J. Bucay, P. A. Deymier, A. Shelke, K. Muralidharan, B. Merheb, J. O. Vasseur, A. Sukhovich, J. H. Page, *Phys. Rev. B* **2011**, *83*, 224301.

[6] M. Molerón, C. Daraio, *Nat. Commun.* **2015**, *6*, 8037.

[7] Y. Wang, B. Yousefzadeh, H. Chen, H. Nassar, G. Huang, C. Daraio, *Phys. Rev. Lett.* **2018**, *121*, 194301.

[8] H. H. Huang, C. T. Sun, *New J. Phys.* **2009**, *11*, 013003.

[9] Z. Yang, H. M. Dai, N. H. Chan, G. C. Ma, P. Sheng, *Appl. Phys. Lett.* **2010**, *96*, 041906.

[10] C. J. Naify, C.-M. Chang, G. Mcknight, S. Nutt, *J. Appl. Phys.* **2010**, *108*, 114905.

[11] M. Yang, G. Ma, Z. Yang, P. Sheng, *Phys. Rev. Lett.* **2013**, *110*, 134301.

[12] N. Fang, D. Xi, J. Xu, M. Ambati, W. Srituravanich, C. Sun, X. Zhang, *Nat. Mater.* **2006**, *5*, 452.

[13] S. Zhang, L. Yin, N. Fang, *Phys. Rev. Lett.* **2009**, *102*, 194301.

[14] H. Jia, M. Ke, R. Hao, Y. Ye, F. Liu, Z. Liu, *Appl. Phys. Lett.* **2010**, *97*, 173507.

[15] J. Zhu, J. Christensen, J. Jung, L. Martin-Moreno, X. Yin, L. Fok, X. Zhang, F. J. Garcia-Vidal, *Nat. Phys.* **2011**, *7*, 52.

[16] Y. Cheng, F. Yang, J. Y. Xu, X. J. Liu, *Appl. Phys. Lett.* **2008**, *92*, 151913.

[17] L. Zhao, E. Laredo, O. Ryan, A. Yazdkhasti, H.-T. Kim, R. Ganye, T. Horiuchi, M. Yu, *Appl. Phys. Lett.* **2020**, *116*, 071902.

[18] D. Lee, C. Cho, J. Mun, N. Park, J. Rho, *Appl. Phys. Lett.* **2018**, *113*, 161904.

[19] S. A. Cummer, J. Christensen, A. Alù, *Nat. Rev. Mater.* **2016**, *1*, 16001.

[20] T. Münzel, M. Sørensen, A. Daiber, *Nat. Rev. Cardiol.* **2021**, *18*, 619.

[21] S.-Y. Li, T.-J. Wang, S. F. V. Wu, S.-Y. Liang, H.-H. Tung, *J. Clin. Nurs.* **2011**, *20*, 396.

[22] A. A. Sayılan, N. Kulakaç, S. Sayılan, *Nurs. Crit. Care* **2021**, *26*, 79.

[23] S. J. Elliott, P. A. Nelson, *IEEE Signal Process. Mag.* **1993**, *10*, 12.

[24] S. Bianchi, A. Corsini, A. G. Sheard, *J. Eng. Gas Turbines Power* **2013**, *136*, 044001.

[25] X. Xu, X. Wang, Y. Mei, *IOP Conf. Ser.: Mater. Sci. Eng.* **2019**, *569*, 032040.

[26] D. Wu, N. Zhang, C. M. Mak, C. Cai, *Appl. Acoust.* **2019**, *143*, 31.

[27] J. Hsu, K. Ahuja, *AIAA 1996-1675, Aeroacoustics Conference* **1996**.

[28] X. Jiang, Y. Li, L. Zhang, *J. Acoust. Soc. Am.* **1995**, *97*, EL363.

[29] D. P. Elford, L. Chalmers, F. V. Kusmartsev, G. M. Swallowe, *J. Acoust. Soc. Am.* **2011**, *130*, 2746.

[30] Y. Zhu, B. Assouar, *Phys. Rev. B* **2019**, *99*, 174109.

[31] C. Cai, C. M. Mak, *J. Acoust. Soc. Am.* **2016**, *140*, EL471.

[32] J. Fey, W. M. Robertson, *J. Appl. Phys.* **2011**, *109*, 114903.

[33] M. B. Xu, A. Selamet, H. Kim, *Appl. Acoust.* **2010**, *71*, 822.

[34] A. Selamet, M. B. Xu, I.-J. Lee, N. T. Huff, *J. Acoust. Soc. Am.* **1989**, *117*, 725.

[35] N. Sugimoto, H. Imahori, *J. Fluid Mech.* **2005**, *546*, 89.

[36] S.-H. Park, *J. Sound Vib.* **2013**, *332*, 4895.

[37] D. E. Spiel, *J. Geophys. Res.* **1992**, *97*, 11443.

[38] C. Cai, C.-M. Mak, X. Shi, *Appl. Acoust.* **2017**, *115*, 74.

[39] F. Lemoult, M. Fink, G. Lerosey, *Phys. Rev. Lett.* **2011**, *107*, 064301.

[40] J. R. Koza, *Genetic Programming: On the Programming of Computers by Means of Natural Selection*, MIT Press, Cambridge **1992**.

[41] J. O. Vasseur, P. A. Deymier, G. Frantziskonis, G. Hong, B. Djafari-Rouhani, L. Dobrzynski, *J. Phys.: Condens. Matter* **1998**, *10*, 6051.

[42] J. O. Vasseur, P. A. Deymier, B. Chenni, B. Djafari-Rouhani, L. Dobrzynski, D. Prevost, *Phys. Rev. Lett.* **2001**, *86*, 3012.

[43] Y. Pennec, J. O. Vasseur, B. Djafari-Rouhani, L. Dobrzyński, P. A. Deymier, *Surf. Sci. Rep.* **2010**, *65*, 229.